Dependency of Particle Size Distribution at Dust Emission on Friction Velocity and Atmospheric Boundary-Layer Stability

Yaping Shao[1], Jie Zhang[2], Masahide Ishizuka[3], Masao Mikami[4], John Leys[5, 6], Ning Huang[2]

[1] Institute for Geophysics and Meteorology, University of Cologne, Germany
[2] Key Laboratory of Mechanics on Disaster and Environment in Western China, Lanzhou University, China
[3] Faculty of Engineering and Design, Kagawa University, Japan
[4] Office of Climate and Environmental Research Promotion, Japan Meteorological Business Support Center, Japan
[5] Department of Planning, Industry and Environment, New South Wales, Australia
[6] The Fenner School of Environment & Society, The Australian National University, Australia

Correspondence to: Jie Zhang (zhang-j@lzu.edu.cn) and Ning Huang (huangn@lzu.edu.cn)

Abstract. Particle size distribution of dust at emission (dust PSD) is an essential quantity to be estimated in dust studies. It has been recognized in earlier research that dust PSD is dependent on soil properties (e.g. whether soil is sand or clay) and friction velocity, u_*, a surrogate for surface shear stress and descriptor for saltation bombardment intensity. This recognition has been challenged in some recent papers, causing a debate on whether dust PSD is "invariant" and the search for its justification. In this paper, we analyse dust PSD measured in the Japan-Australian Dust Experiment and show that dust PSD is dependent on u_* and on atmospheric boundary-layer (ABL) stability. By simple theoretical and numerical analysis, we explain the two reasons for the latter dependency, both related to enhanced saltation bombardment in convective turbulent flows. First, u_* is stochastic and its probability distribution profoundly influences the magnitude of the mean saltation flux due to the non-linear relationship between saltation flux and u_*. Second, in unstable conditions, turbulence is usually stronger, which leads to higher saltation-bombardment intensity. This study confirms that dust PSD depends on u_*, and more precisely, on the probability distribution of u_*, which in turn is dependent on ABL stability, and consequently dust PSD is also dependent on ABL. We also show that the dependency of dust PSD on u_* and ABL stability is made complicated by soil surface conditions. In general, our analysis reinforces the basic conceptual understanding that dust PSD depends on saltation bombardment and inter-particle cohesion.

1 Introduction

Gillette (1981) explained that dust emission can be produced by aerodynamic lift and saltation bombardment, but under realistic wind, aerodynamic-lift emission is much weaker than saltation-bombardment emission. This hypothesis was confirmed by Shao et al. (1993). It is recognized that saltation bombardment is the most important mechanism for dust emission, and dust emission rate, F, is proportional to streamwise saltation flux, Q[1].

Rice et al. (1995, 1996) visualized the process of saltation bombardment using wind-tunnel photos: a saltation particle at impact on surface ejects a tiny amount of soil into air, leaving behind a crater. Models for estimating crater size have been developed by, e.g., Lu and Shao (1999). The fraction of dust that gets emitted from the ejection is difficult to estimate, because it depends both on inter-particle cohesion and bombardment intensity. Since inter-particle cohesion depends on particle size, d, the fraction of dust emitted must also depend on d. Thus, for a given soil, the particle size distribution of dust at emission (emission-dust PSD), $p_s(d)$, must depend on saltation bombardment or on friction velocity, u_* ($\sqrt{\tau}/\rho$ with τ being surface shear stress and ρ air density; see Section 4.2 for discussion). Alfaro et al. (1997) confirmed that $p_s(d)$ depends on u_*: as u_* increases, $p_s(d)$ shows a higher fraction of dust of smaller d. Based on this result and the observations that different laboratory techniques for PSD analysis yield profoundly different outcomes, depending on the disturbances applied to the samples (Figure 1), Shao (2001) suggested to use a minimally-disturbed PSD, $p_m(d)$, as the limit of $p_s(d)$ for weak saltation, and a fully-disturbed PSD, $p_f(d)$, as the limit of $p_s(d)$ for strong saltation. In this way, $p_s(d)$ is approximated as a weighted average of $p_m(d)$ and $p_f(d)$, namely,

$$p_s(d) = \gamma p_m(d) + (1 - \gamma)p_f(d) \tag{1}$$

where $0 \leq \gamma \leq 1$ is an empirical function of $u_{*t}(d)$, the threshold friction velocity for particles of size d.

What is emission-dust PSD? We must distinguish three closely related yet subtly different dust PSD, namely, emission-dust PSD, airborne-dust PSD, and emission-flux PSD. PSD of dust in air (airborne-dust PSD) has been collected from different places under different conditions. Emission-dust PSD and airborne-dust PSD are identical, if the latter is measured at dust source at height zero. Airborne-dust PSD can be used to approximate emission-dust PSD if it is measured close to the source and the dependency of particle motion in air on particle size can be neglected. For modelling size-resolved dust concentration in air (i.e. solving the dust concentration equation for different particle sizes), emission-dust PSD offers the Dirichlet-type boundary condition. If size-resolved dust-emission-fluxes can be calculated, then we can specify the Neumann-type boundary condition for solving the dust concentration equation. From size-resolved dust-emission-fluxes, an emission-flux PSD can be calculated (Section 2; Section 4.2). Emission-flux PSD is neither emission-dust nor airborne-dust PSD, but describes how vertical dust-concentration gradient depends on particle size. In some earlier publications, unfortunately, the differences between the three dust PSDs are not clearly explained.

---

[1]The ratio $\gamma_b = F/Q$ is a main issue of dust emission studies (Zender et al., 2003; Laurent et al., 2006). Marticorena et al. (1997) showed that γ_b depends on soil clay content. Shao (2004) suggested that γ_b depends on friction velocity, soil type and soil particle size distribution.

To our knowledge, emission-dust PSD has never been directly measured, but approximated using airborne-dust PSD measured at some, often different, heights (e.g. Kok, 2011b, Table S1). Available data of airborne-dust PSDs give the impression that they do not differ much. It has thus been suggested that airborne-dust PSDs may be "not-so-different" and hence emission-dust PSDs may also be "not-so-different". Reid et al. (2008) stated that "on regional scales, common mode dust is not functionally impacted by production wind speed, but rather influenced by soil properties such as geomorphology …". Kok (2011a, 2011b) proposed a dust emission model by treating dust emission as a process of aggregate fragmentation by saltation bombardment. Since aggregate fragmentation is similar to brittle fragmentation, the size distribution produced in the process is scale-invariant (Astrom, 2006). Kok (2011a, 2011b) then proposed an emission-dust PSD and estimated its parameters from the data listed in Table S1 of Kok (2011b). The proposed emission-dust PSD is frequently used in dust models (Giorgi et al., 2012; Albani et al., 2014; Pisso et al., 2019). However, whether the "not-so-different" airborne-dust PSDs justify "brittle fragmentation" as the underlying process for dust emission requires scrutiny.

Studies on dust PSD are yet to deliver definitive answers. The airborne-dust PSD measurements of Rosenberg et al. (2014) pointed to larger fraction of fine particles than in earlier published data. Ishizuka et al. (2008) found that airborne-dust PSD measured close to surface depends on u_* for a weakly crusted soil. Sow et al. (2009) examined the dependency of emission-flux PSD on u_* for three dust events and reported that the PSD appeared to be independent on u_*, but differed significantly between weak and strong events. In line with Sow et al. (2009), Khalfallah et al. (2020) reported that emission-flux PSD depends on atmospheric boundary-layer (ABL) stability, and attributed this to the dependency of particle diffusivity on particle size. They stated that the dependency of emission-dust PSD on u_*, as observed by Alfaro et al. (1997), may be of secondary importance in natural conditions compared to its dependency on ABL stability.

The argument of Khalfallah et al. (2020) rests on the preferential particle diffusion in turbulent flows. Csanady (1963) suggested that particle eddy diffusivity, K_p, is related to eddy diffusivity, K, by

$$K_p = K(1 + \beta^2 w_t^2/\sigma^2)^{-1/2} \tag{2}$$

where β is a coefficient, w_t particle terminal velocity and σ the standard deviation of (vertical) turbulent velocity. The analyses of Walklate (1987) and Wang and Stock (1993), among many others, reached similar conclusions. For dust particles smaller than 10μm, K_p/K is close to one for $\sigma = 0.5\text{ms}^{-1}$, and still larger than 0.95 for $\sigma = 0.1\text{ms}^{-1}$ (Shao, 2008; Fig. 8.12). Thus, preferential particle diffusion does not seem to fully explain the dependency of dust PSD on ABL stability.

The confusion surrounding emission-dust PSD prompted us to re-examine the data of Ishizuka et al. (2008) from the Japan-Australian Dust Experiment (JADE). In JADE, airborne-dust PSD were measured at small height directly above the dust source and can be assumed to well approximate the emission-dust PSD. By composite analysis for different u_* and ABL stabilities, we show that dust PSD depends on u_*, supporting the findings of Alfaro et al. (1997), and depends on ABL stability, consistent with the findings of Khalfallah et al. (2020). But in contrast to Khalfallah et al. (2020), we argue that

90 these dependencies are not mutually exclusive, but collectively point to the simple physics that emission-dust PSD is
91 dependent on saltation-bombardment intensity and efficiency.

2 JADE Data

93 JADE was carried out during 23 Feb ~ 14 Mar 2006 on an Australian farm at (33°50'42.4"S, 142°44'9.0"E) (Ishizuka et al.,
94 2008, 2014). The 4 km^2 farmland was flat and homogeneous such that the JADE data are not affected by fetch. In JADE,
95 atmospheric variables, land surface properties, soil PSD, size-resolved sand fluxes and dust concentrations were measured.
96 Size-resolved dust-emission fluxes were estimated from the dust concentration measurements. Three Sand Particle Counters
97 (SPCs) (Mikami et al., 2005) were used to measure the sand fluxes in the size range of 39 - 654 μm in 32 bins at 0.05, 0.1
98 and 0.3 m above ground at a sampling rate of 1 Hz. Using the sand fluxes, q_j (j = 1, 32), the PSD of saltation particles
99 (saltation-flux PSD) is estimated for a particle size bin at d_j with bin size Δd_j as

$$p(d_j)\Delta d_j = q_j / \sum_{j=1}^{j=32} q_j \qquad (2)$$

101 Dust concentration was measured using Optical Particle Counters (OPC) for 8 size groups: 0.3 – 0.6, 0.6 – 0.9, 0.9 – 1.4,
102 1.4 – 2.0, 2.0 – 3.5, 3.5 – 5.9, 5.9 – 8.4 and 8.4 – 12.0μm at 1, 2 and 3.5m above ground. The upper size limit for the last bin
103 is not well defined, but set empirically to 12.0μm such that this bin can still be included in the analysis. Airborne-dust PSD is
104 estimated as

$$p(d_j)\Delta d_j = c_j / \sum c_j \qquad (3)$$

106 where c_j denotes the dust concentration for size bin j. Similarly, the emission-flux PSD can be defined as

$$p(d_j)\Delta d_j = F_j / \sum F_j \qquad (3a)$$

108 where F_j denotes the dust flux for size bin j. It should be noted that the emission-flux PSD describes how the covariance of
109 particle-velocity and particle-concentration depends on particle size, not the concentration itself. In this study, we use the
110 airborne-dust PSD observed at 1m to approximate emission-dust PSD, and use the airborne-dust PSD observed at 3.5m and
111 the emission-flux PSD derived from the 3.5m- and 1m-OPC measurements for additional discussions (Section 4.2).
112 Hereafter, emission-dust PSD approximated using the 1m-OPC airborne-dust PSD is simply referred to as dust PSD, unless
113 otherwise explicitly stated.
114 Atmospheric variables, including wind speed, air temperature and humidity at various levels, radiation and precipitation
115 were measured using an automatic weather station. These quantities were sampled at 5-second intervals and their 1-minute
116 averages were recorded (see Section 4.2 for discussions). Two anemometers mounted at 0.53 and 2.16m measured wind

117   speed. From the atmospheric data, the Obukhov length, L, sensible heat flux, H, and friction velocity, u_*, were derived.[2] Also

118   measured were soil temperature and moisture.
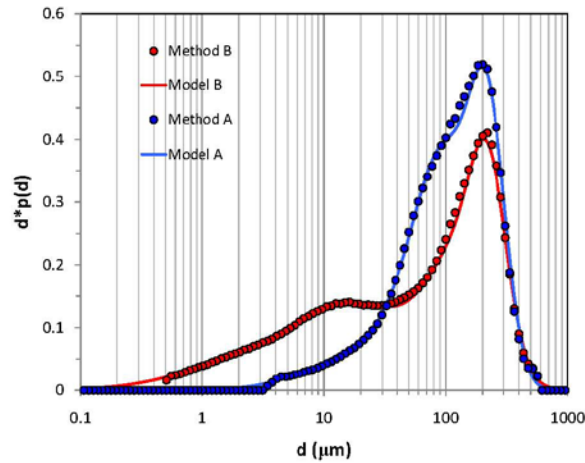
119

120   Figure 1. Soil particle-size distribution obtained using Method A and Method B, together with the respective approximations (Model A

121   and Model B).

122   Surface soil samples were taken and soil PSD was analysed in laboratory using Method A and B with a particle size

123   analyser (Microtrac MT3300EX, Nikkiso). In Method A, water was used for sample dispersion with no ultrasonic action. In

124   Method B, sodium hexametaphosphate (HMP) 0.2% solution was used for sample dispersion and 1-minute ultrasonic action

125   of 40W was applied. Following the convention of sedimentology, the soil is a sandy loam based on the analysis using

126   Method B. Figure 1 shows $p_A(d)$ (soil PSD from Method A) and $p_B(d)$ (soil PSD from Method B) and the corresponding

127   approximations: p_A shows a larger fraction of particles in the range of 30~300µm, while p_B a larger fraction of particles in the

128   range of 0.1~30µm.

129   An overview of the JADE data is shown in Figure 2. During the experiment, 12 significant aeolian events were recorded,

130   as marked in the figure. Most of the events occurred under unstable ABL conditions. Several quantities can be used as a

131   measure of ABL stability, but the one used here is the convective scaling velocity, w_*, defined as

132
$$w_* = \left(\frac{g}{\bar{\theta}} H_0 z_l\right)^{\frac{1}{3}} \tag{4}$$

133   where $g/\bar{\theta}$ is the buoyancy parameter with g being the acceleration due to gravity and $\bar{\theta}$ the mean potential temperature; H_0 is

134   surface kinematic heat flux (Kms^{-1}) and z_l a scaling length (set to the capping inversion height for convective ABL and 100m

135   for stable ABL). For unstable conditions, w_* is positive while for stable conditions w_* is negative. The reason for choosing w_*

---

[2] Drag-partition theory (Raupach, 1992; Webb et al., 2020) tells that shear stress, $\tau = \rho u_*^2$, is not the same as the shear stress, τ_s, experienced by soil particles, due to roughness sheltering. For JADE, the surface is bare and thus the effect of roughness sheltering is neglected. The saltation fluxes used in this study are measured and do not involve the assumption $\tau = \tau_s$ or otherwise.

136 is that it is a scaling parameter for the strength of turbulence. Usually, w_* is not used for stable ABLs, but is used here as an
137 indicator for the suppression of turbulence by negative buoyancy.

138   In addition to the 12 events, a number of weak and intermittent events occurred. In this study, we first use the whole
139 dataset for dust PSD analysis, and then use the data for Event-10, 11 and 12 for case studies. These three events are chosen
140 for that Event-10 is the strongest event during JADE, Event-11 is one that occurred at night under stable conditions, while
141 Event-12 occurred with a weakly crusted soil surface (Ishizuka et al., 2008).

142
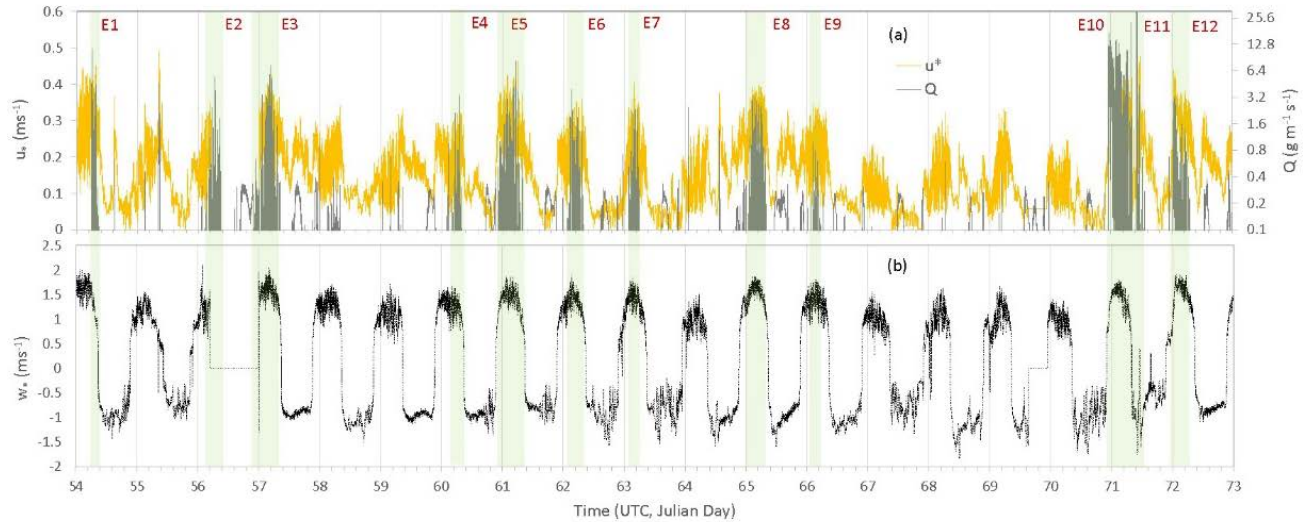
143
144 Figure 2. (a) One-minute averaged friction velocity, u_*, and streamwise saltation flux, Q, for the JADE observation time period; (b) One-
145 minute averaged convective scaling velocity, w_*. In addition to the 12 aeolian events marked, a number of weaker and intermittent aeolian
146 events occurred.

147 **3 Results**

148 **3.1 Overall Results**

149
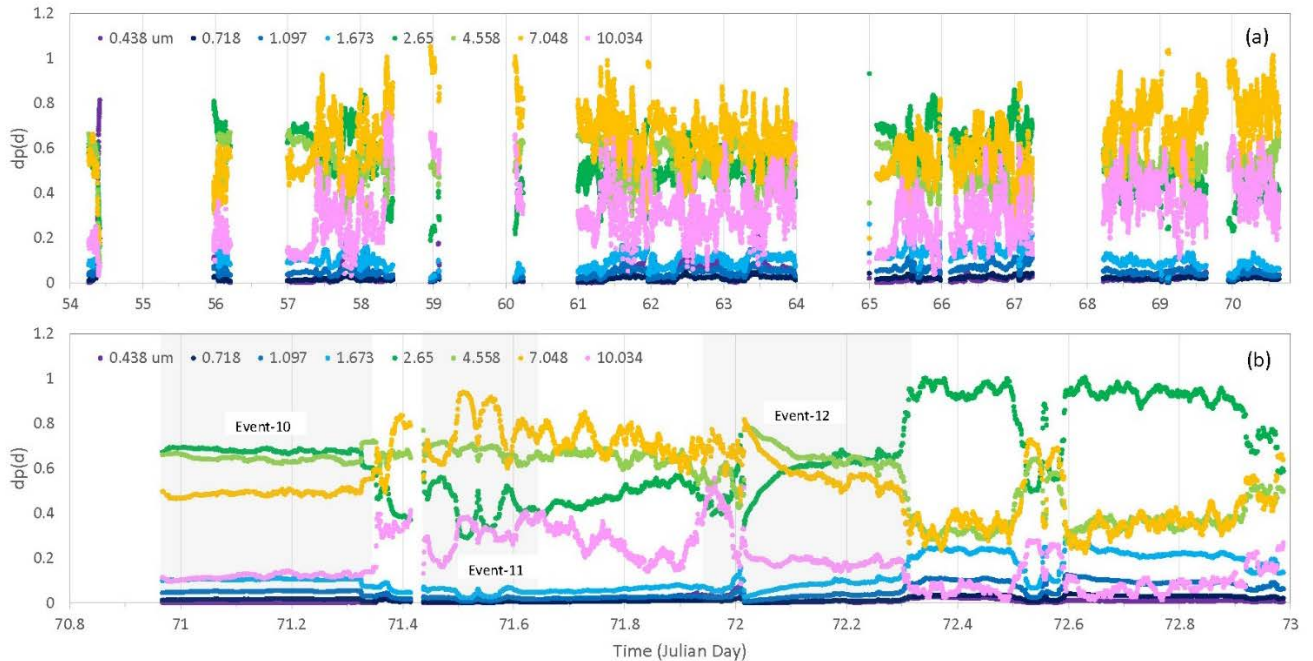
Figure 3. Dust PSD measured at 1m using OPC for the entire JADE observation period plotted in two sections, (a) for section Julian day 54 ~ 70.8 and (b) for section Julian day 70.8 ~ 73.0.

Plotted in Figure 3 are the time series of dust PSD for the entire JADE period, which show rich temporal variations, probably apart from Event-10. To examine dust-PSD dependency on friction velocity, we use u_* to denote the one-minute values of friction velocity, $p(u_*)$ its probability density function (PDF), $\bar{u}_*$ its mean and σ_{u*} its standard deviation. The u_* values are divided into the categories of 0~0.25, 0.25~0.35, 0.35~0.45 and 0.45~0.55 ms^{-1}, and the corresponding dust PSDs and saltation PSDs are sorted accordingly. These u_* categories correspond roughly to intermittent, weak, moderate and strong saltation, respectively. The threshold friction velocity, u_{*t}, for the JADE site is around 0.2ms^{-1}, but intermittent saltation has been observed oft at u_* below this u_{*t}. The dust PSDs are then composite averaged for the u_* categories. Figure 4a shows the dust PSDs for the different u_* categories and the mean dust PSD, i.e., dust PSD averaged over all u_* categories (including a total of 15634 one-minute points). We have repeated the same averaging procedure using a subset of the JADE data, conditioned with $Q > 0.1$gm^{-1}s^{-1} and found that the results are very similar to those presented in Figure 4. The mean dust PSD shows an interesting local minimal at ~ 4μm. This is attributed to the lack of particles of this size in the $u_* <$ 0.25ms^{-1} category. Figure 4a shows that dust PSD clearly depends on u_*, particularly in the size range 2~10μm. In general, as u_* increases, the fraction of fine dust particles increases. For the submicron size range, the dependency of dust PSD on u_* is less definitive. The dust PSD for the $u_* < 0.25$ ms^{-1} category shows a higher fraction of submicron dust particles, especially in stable conditions (Figure 4b). Apart from this, the results shown in Figure 4a are consistent with the findings of Alfaro et al. (1997) that dust PSD is u_* dependent.

168
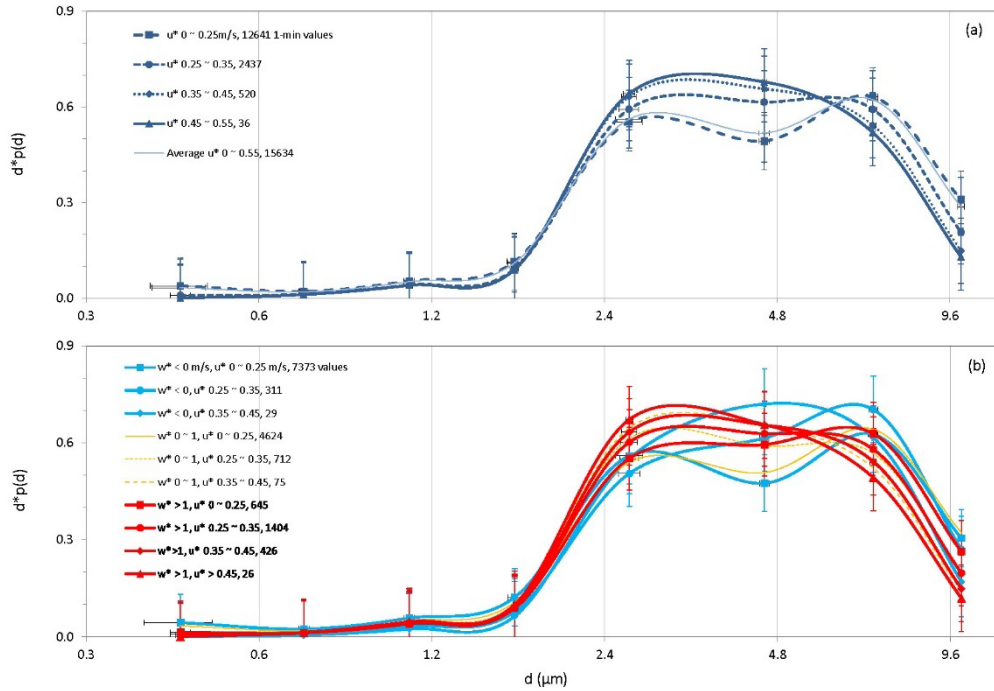
Figure 4. (a) Dust PSD for different u_* categories derived from the whole JADE dataset; (b) as (a), but for the different u_*
categories under stable ($w_* < 0$), moderately unstable ($0 \le w_* < 1$ ms^{-1}) and unstable ($w_* \ge 1$ ms^{-1}) conditions.

171

To examine the dust PSD dependency on ABL stability, we divide the dataset into three, namely, stable ($w_* < 0$),
moderately unstable ($0 \le w_* < 1$ms^{-1}) and unstable ($w_* \ge 1$ ms^{-1}) stability classes. For each stability class, the dust PSD data
are regrouped according to the u_* categories. Figure 4b shows the dust PSDs averaged for different u_* categories and stability
classes. For given stability class, dust PSD shows dependency on u_*, and for a given u_* category, dust PSD shows
dependency on w_*. For given u_*, the mode of dust PSD shifts systematically to finer particles as the ABL becomes more
unstable.

178

3.2 Case Study Results

We now study the cases of Event-10 (09:49~19:13 12 Mar 2006; Julian Day 70.9506940~71.3423611), Event-11 (21:12
12 Mar ~ 02:08 13 Mar 2006, Julian Day 71.42500~71.63056) and Event-12 (09:54~18:58 13 Mar 2006, Julian Day
71.95417~72.33194). Figure 5 shows the one-minute averages of wind speed at 0.53m, U, air temperature at 0.66m, T,
saltation flux at 0.05m, q_{5cm}, and dust concentration (summed over all particle size bins) at 1m, C_{1m}. Event-10 occurred under
daytime unstable conditions. It was a very hot day prior to a cool change (cold front causing temperature drop but no
rainfall), with near surface air temperature reaching 52°C and wind speed ~8ms^{-1}. The event lasted ~10 hours. The cool
change occurred at ~19:00-21:00 13 Mar 2006 local time. While precipitation was not recorded by the rain gauge (with

187 resolution of 0.2 mm), the rain sensor [PPS-01(C-PD1), PREDE Co. Ltd.], as marked in Figure 5b, sensed an event of
188 raindrops shortly before the cool change, lasting about two minutes, and shortly after, lasting about one minute (Ishizuka et
189 al., 2008). The strong winds (probably also strong sand drift and dust emission) accompanying the cool change caused the
190 shutdown of the instruments and thus, unfortunately, this period was not fully recorded. Event-11 occurred under stable
191 conditions after the cool change in the night time of 12/13 Mar 2006, during which T was dropping from ~40°C to ~33°C and
192 U from ~8ms^{-1} to ~5ms^{-1}. Event-11, which can also arguably be considered to be part of Event-10, was much weaker than
193 Event-10.

194   As the OPC measurements were taken close to the surface and directly above the dust source, the dust-concentration
195 values were generally high. For Event-10, the mean, standard deviation, maximum and minimum of C_{1m} are respectively
196 7.56, 8.56, 65.96 and 0.02 mg m^{-3}, and for Event-11 3.05, 10.57, 100.17 and 0.04 mg m^{-3}. The extremely high dust
197 concentrations measured shortly before and after the cool change could be affected by dust advection and are excluded from
198 the analysis (although their inclusion made no difference to the event averages of the dust PSDs). For other times, it can be
199 safely assumed that the dust observed was locally emitted.

200
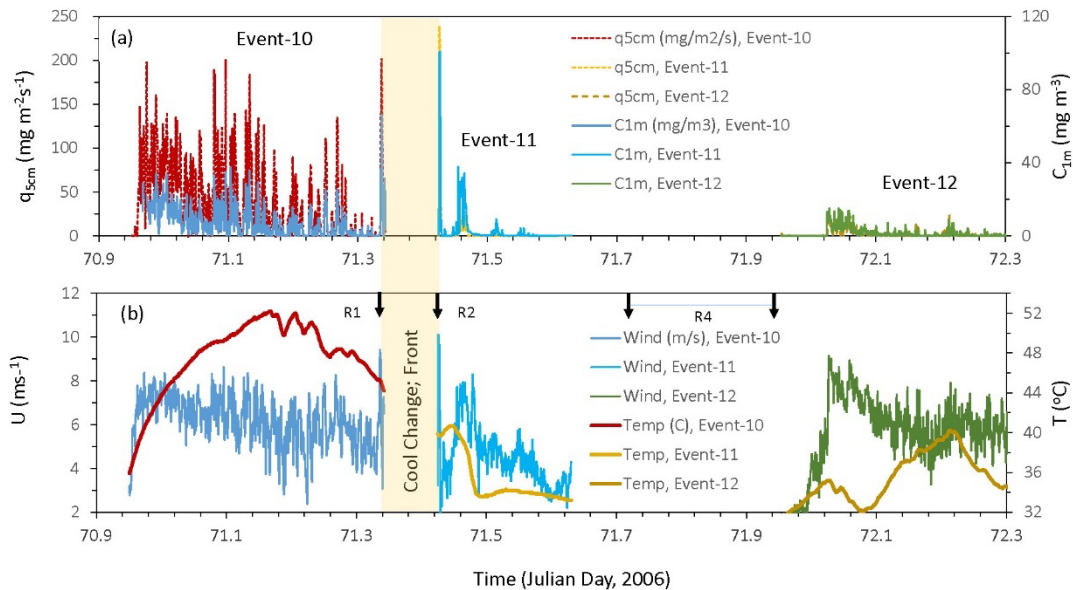
201

202 Figure 5. (a) one-minute averaged saltation flux at 0.05m, q_{5cm}, and dust concentration at 1m, C_{1m}, for Event-10, -11 and 12;
203 (b) as (a) but for wind speed at 0.53m above ground, U, and air temperature at 0.66m, T. The cool change is marked and the
204 three rain events sensed by the rain sensor are marked as R1, R2 and R4 using the black arrows.

205

206   Event-12 is developed shortly after the weak rainfall event (R4). Again, while precipitation was not recorded by the rain
207 gauge (i.e. total rainfall was less than 0.2 mm), the rain sensor reported rain drops during 71.70625~71.95278. Ishizuka et al.

208   (2008) reported that Event-12 is unique for JADE, because it is the only case when the soil surface was weakly crusted. We
209   will show later how dust PSD can substantially evolve even within one dust event, as soil surface conditions change (Figure
210   10).
211
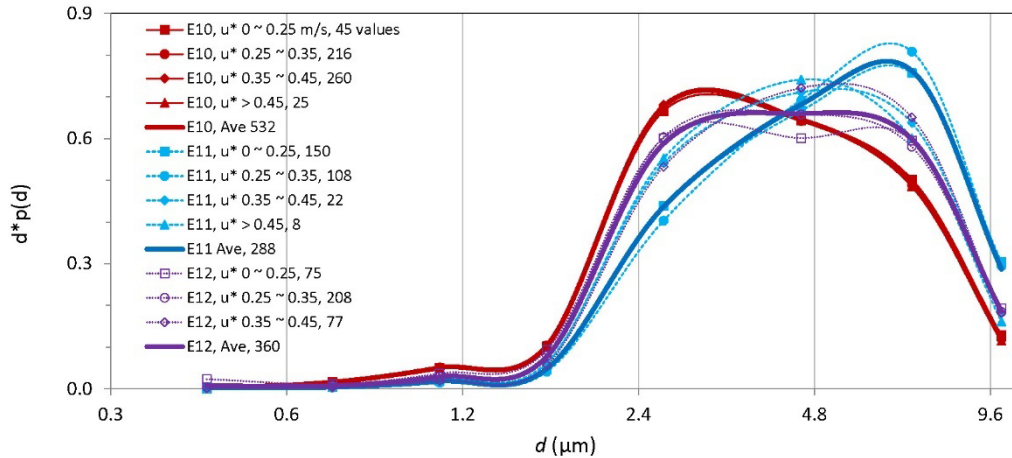
213   Figure 6. Dust PSD for different u_* categories for Event-10, 11 and 12. Also shown are the PSDs averaged over all u_* categories for the
214   individual events.

215   Figure 6 shows the dust PSDs for the different u_* categories for Event-10, 11 and 12. For Event-11 and 12, the
216   dependency of dust PSD on u_* is obvious, in agreement with the overall results shown in Figure 4a. The dust PSD for Event-
217   10 shows no clear dependency on u_*, an observation also reported in Shao et al. (2011). Our basic argument for dust PSD
218   dependency on u_* rests upon the assumption that saltation-impact speed is u_* dependent. It has been suggested that impact-
219   particle speed may not strongly depend on u_* for transport-limited saltation (Ungar and Haff, 1987), because particle-flow
220   feedbacks force an approximately constant saltation-impact speed. While this argument is supported by some experimental
221   evidence (Martin and Kok, 2017) and numerical simulations (Duran et al., 2012; Kok et al., 2012), its general validity and
222   the conditions for its validity need further examination. JADE Event-10 is probably a case which comes closest to meet the
223   requirements of strong particle-flow feedback and sustained equilibrium of saltation for the Ungar and Haff (1987)
224   hypothesis to apply. In addition, Event-10 occurred on an extremely hot and dry day, with the 0.66m air temperature
225   reaching ~52$^{\mathrm{o}}$C and the 0.66m relative humidity dropped below 3%. It is likely that under such extreme weather conditions,
226   the inter-particle cohesion is destroyed. These factors combined may be responsible for the lack of dust PSD dependency on
227   u_* for Event-10 (Figure 6). But for all other JADE events, the dependency of dust PSD on u_* is significant.
228   The event-averaged dust PSDs for Event-10, -11 and -12 clearly differ. For Event-10, the mean and standard deviation of
229   u_* and w_* were respectively (0.36, 0.057) and (1.03, 0.29), all in ms^{-1}, and for Event-11 (0.28, 0.077) and (-0.41, 0.159).
230   From Event-10 to -11, the dust PSD mode shifted from about 3µm to 6µm. During Event-10, a substantially higher fraction
231   of particles in the size range of 0.4 ~ 4µm exists. To further examine how dust PSD depends on saltation intensity, we have

averaged the dust PSDs for different Q categories (not shown). It is found that weak saltation corresponded to coarser dust particles and strong saltation to finer dust particles. The results shown in Figure 6 confirm the dependency of dust PSD on ABL stability, consistent with the overall results shown in Figure 4.

Figure 5b shows that the wind conditions for Event-10 and Event-12 were not too different, but Event-12 was much weaker. Figure 6 shows that also the dust PSDs for the two events considerably differ, with Event-10 being the one with richer finer dust particles. Event-12 will be further discussed in Section 4.2.

We make the following observations based on the JADE data: (1) Dust PSD has rich temporal variations and is not "universal"; (2) Dust PSD depends on u_* and ABL stability; and (3) Dust PSD is influenced by soil surface conditions. These observations support the conceptual understanding that dust PSD is determined both by saltation bombardment and by soil binding strength (Shao, 2001, 2004).

4 Discussions

4.1 Influence of Turbulence on dust PSD

The reason for the dependency of dust PSD on u_* has been explained in Gillette et al. (1974), Gillette (1981), Shao et al. (1993), Alfaro et al. (1997) and Shao (2001), because u_* is a descriptor of saltation bombardment intensity. In the earlier explanations, only mean friction velocity and mean saltation are considered, while the turbulent nature of saltation bombardment is implicitly neglected. But how is the dependency of dust PSD on ABL stability, here w_*, explained? The most conspicuous reason is the enhanced saltation bombardment by turbulence in unstable conditions.
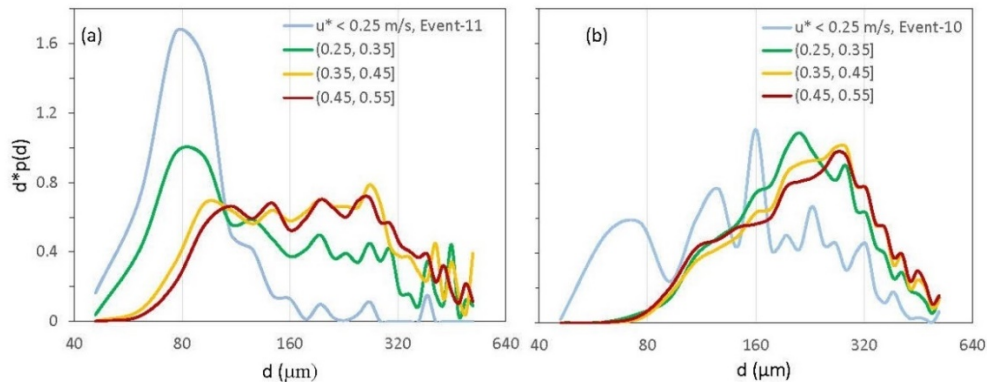
Figure 7. (a) Saltation PSD averaged for four different u_* categories for Event-11; (b) as (a), but for Event-10.

It is interesting to examine how dust PSD is related to saltation PSD. The saltation PSD for Event-10 and -11 are shown in Figure 7. First, for $u_* \leq 0.25 \text{ms}^{-1}$ in Event-11, saltation PSD was confined to a narrow size range centred at 70~80µm where

253 u_{*t} is minimum. This indicates that saltation splash/bombardment was weak to mobilize particles in other size ranges. In

254 contrast, for $u_* \leq 0.25\text{ms}^{-1}$ in Event-10, saltation PSD covered a broader size range, implying that saltation splash was strong

255 to entrain particles of other sizes. Second, for both Event-10 and -11, the peak values of saltation PSD were shifted to larger

256 particles for larger u_*: for Event-10 the peak for $u_* = 0.35\text{ms}^{-1}$ was at 203.3µm, while for $u_* = 0.55\text{ms}^{-1}$ at 257.8µm. Clearly,

257 since u_{*t} is particle size dependent, saltation PSD is a selective sample of the soil PSD by wind. Third, the saltation PSDs for

258 given u_* categories (e.g., $0.35 < u_* \leq 0.45\text{ms}^{-1}$, Figure 8a and 8b) differed significantly between Event-10 and -11 as a

259 consequence of ABL stability. In Event-11 (Figure 8a), saltation was not fully developed, as the saltation PSD plateau in the

260 size range 100~300µm suggests, implying again that saltation splash/bombardment was not efficient. In Event-10 (Figure

261 7b), saltation was more fully developed.

262   The stronger saltation of Event-10 is partially attributed to the stronger wind and instability, which result in a larger $\bar{u}_*$

263 than in Event-11. It is known from the ABL similarity theory that,

264
$$\bar{u}_* = \frac{kz}{\phi_m}\frac{\partial \bar{u}}{\partial z} \tag{5}$$

265 where κ is the von Karman constant, z height and ϕ_m a similarity function (Stull, 1988):

266
$$\phi_m = \begin{cases} 1 + \beta_m \zeta & \zeta > 0 \text{ stable} \\ (1 - \gamma_m \zeta)^{-1/4} & \zeta < 0 \text{ unstable} \\ 1 & \zeta = 0 \text{ neutral} \end{cases} \tag{6}$$

267 where $\zeta = z/L$ (L is Obukhov length) and $\beta_m = 5$ and $\gamma_m = 16$ are empirical coefficients (Businger et al., 1971). For stable

268 conditions, $\phi_m > 1$ and for unstable conditions $\phi_m < 1$. Figure 8 shows the PDFs of u_* and w_* for Event-10 and -11,

269 together with the approximations for the PDFs of u_*. For Event-10, $\bar{u}_* = 0.37\text{ms}^{-1}$, while for Event-11, $\bar{u}_* = 0.28\text{ms}^{-1}$.

270
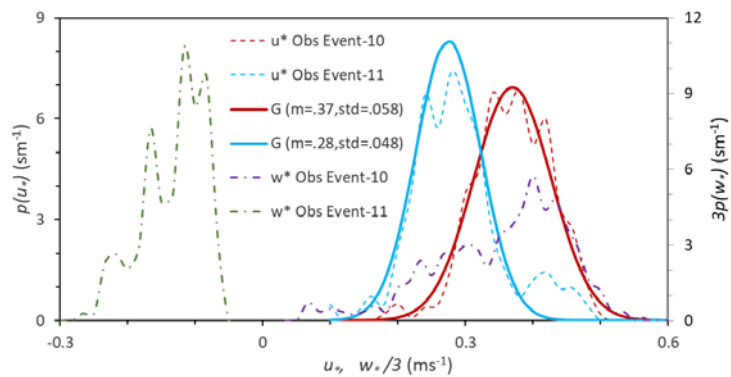
Figure 8. The probability density functions of u_* and w_*, $p(u_*)$ and $p(w_*)$, respectively, for Event-10 and -11, together with the Gaussian approximations for the $p(u_*)$ functions. The mean values (m) and standard deviations (std) for the Gaussian (G) distributions are given. Note that for $p(w_*)$, $3p(w_*)$ against $w_*/3$ is plotted to conveniently present the information in the same graph.

We suggest that the dependency of dust PSD on w_* for given u_* is attributed to saltation bombardment intensity from two perspectives. First, as Figure 8 shows, u_* is a stochastic variable. Li et al. (2020) suggested that $\tau = \rho u_*^2$ in neutral conditions is Gauss distributed. Klose et al. (2014) reported that τ in unstable conditions is Weibull distributed. The exact form of $p(\tau)$ requires further investigation, but the JADE data of u_* show that $p(u_*)$ is reasonably Gaussian. Hence,

$$p(\tau) = \frac{1}{2\rho u_*} p(u_*) \tag{7}$$

is skewed to smaller τ, suggesting that the large-eddy model results of Klose et al. (2014) are qualitatively reasonable. Figure 8 shows that u_* in Event-10 not only had a larger mean value but also a larger variance than in Event-11. We emphasize that the variance of u_* strongly affects saltation, because saltation flux depends non-linearly on u_*. To illustrate this, we consider u_{*1} and u_{*2}, and assume that

- u_{*1} and u_{*2} are Gaussian distributed and have the same mean that equals u_{*t} (say 0.2ms^{-1})
- u_{*1} and u_{*2} have respectively standard deviation, σ_1 and σ_2, with $\sigma_2 = \eta\,\sigma_1$ and $\eta > 1$; and
- Q satisfies the Owen's model (Owen, 1964),

$$Q_i = c u_{*i}^3 \left(1 - \frac{u_{*t}^2}{u_{*i}^2}\right) \qquad \text{for } u_* > u_{*t};$$

$$\text{otherwise } 0; \quad \text{with } i = 1, 2 \tag{8}$$

where c is a dimensional constant. It follows that the ratio of the mean values of Q_2 and Q_1 is

$$\eta_Q = \frac{\bar{Q}_2}{\bar{Q}_2} = \int_{u_{*t}}^{\infty} Q_2\, p(u_{*2}) du_{*2} \Big/ \int_{u_{*t}}^{\infty} Q_1\, p(u_{*1}) du_{*1} \tag{9}$$

Equation (9) can be evaluated numerically for different η (Table 1) and is approximately

$$\eta_Q = 0.607\, \eta^2 - 0.0028\eta + 0.4283 \tag{10}$$

This shows that $p(u_*)$ profoundly influences the magnitude of Q. For fixed $\bar{u}_*$, a larger u_* variance corresponds to a larger $\bar{Q}$.

Table1. Streamwise saltation flux ratios, η_Q, for different u_* std ratios, η (see text for details).

η	1.2	1.4	1.6	1.8	2	3	4
η_Q	1.30	1.63	2.00	2.41	2.86	5.83	10.15

294   Second, in unstable conditions, turbulence is stronger due to buoyancy production, which leads to increased saltation

295   bombardment intensity. We do not have independent evidence to verify this, but to illustrate the point, we use a two-

296   dimensional (2-d, x_1 in mean wind direction and $x_3 \equiv z$ in vertical direction) saltation model (Supplement A) to simulate the

297   impact kinetic energy of saltation sand grains. For given u_* and roughness length, z_0, a 2-d turbulent flow is generated with

298   the mean wind assumed to be logarithmic $\kappa \overline{u_1} = \overline{u_*} \ln(z/z_0)$ and the velocity standard deviations satisfy

299
$$\frac{\sigma_{u1}}{\overline{u}_*} = a \cdot ln\left(\frac{z}{z_0}\right) \tag{11}$$

300
$$\frac{\sigma_{u3}}{\overline{u}_*} = f_{u3}(\zeta) \cdot a \cdot ln\left(\frac{z}{z_0}\right) \tag{12}$$

301   and the dissipation rate for turbulent kinetic energy, ε, satisfies

302
$$\varepsilon \frac{\kappa z}{\overline{u}_*^3} = f_\varepsilon(\zeta) \tag{13}$$

303   The similarity relationships $f_{u3}(\zeta)$ and $f_\varepsilon(\zeta)$ follow Kaimal and Finnigan (p16, 1995). As saltation takes place in the layer

304   close to the surface, the vertical profiles of σ_{u1} and σ_{u3} are considered following Yahaya et al. (2003). The coefficient a

305   (=1.16β) is varied by setting β to 0.75, 1.00 and 1.25 for weak, normal and strong turbulence, respectively.

306   In each numerical experiment, 20000 sand grains of identical size are released from the surface and their trajectories are

307   computed. At impact on the surface, the particles rebound with a probability of 0.95 and a rebounding kinetic energy, K_{reb},

308   0.5 times the impact kinetic energy, K_{imp}. The rebound angle is Gauss distributed with a mean of 40° and standard deviation

309   5°. Splash entrainment is neglected. The PDF of K_{imp}, $p(K_{imp})$, is used as a measure for bombardment intensity.

310   Many numerical experiments were carried out, but for our purpose, we show only the results of the ones listed in Table 2.

311   The initial velocity components of sand grains (V_{1o}, V_{3o}) are generated stochastically. V_{1o} is Gauss distributed with a mean

312    $\bar{V}_{1o} = \bar{u}_* \cos(55^o)$ and standard deviation, $\sigma_{V1o} = 0.1\bar{u}_*$. V_{3o} is Weibull distributed with a shape parameter $A = 2$ and a scale

313   parameter $B' = \bar{u}_* \sin(55^o)/\Gamma(1 + 1/A)$ where Γ is a Gamma function. To account for the influence of stability on V_{3o}, B'

314   is modified such that the adjustment to σ_{V3o} is the same as that to $\sigma_{u3}(10z_0)$, i.e., the modified scale parameter, B, is given

315   by

316
$$B = \beta f_{u3}\left(\frac{10z_0}{L}\right) B' \tag{14}$$

317
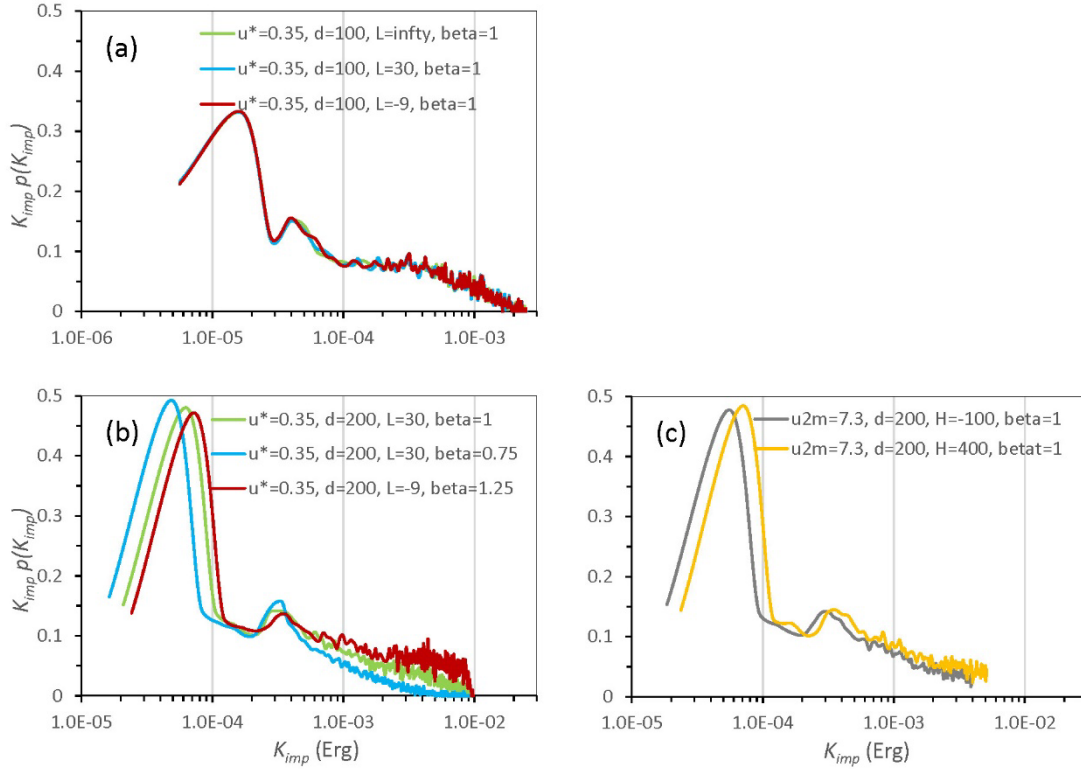
318

319 Figure 9. Probability density function $p(K_{imp})$ (plotted in $K_{imp}\,p(K_{imp})$ against K_{imp} in logarithmic scale) for the numerical experiments. In

320 (a), $p(K_{imp})$ is shown for $u_* = 0.35$ms^{-1}, $d = 100$μm and $\beta = 1$ but for three different Obukhov lengths $L = \infty$, 30m and -9m. In (b), the effect

321 of β on $p(K_{imp})$ is examined; and in (c) the effect of stability on $p(K_{imp})$ with given mean wind speed at $z = 2$m is examined.

322   Figure 9a compares $p(K_{imp})$ for Exp1a, 1b and 1c and shows that $p(K_{imp})$ for these cases is very similar. The small

323 differences in $p(K_{imp})$ between the cases suggest that the differences in particle trajectory arising from the stability

324 modification to turbulence profile, with u_* fixed, are negligible. However, a small change in β, as Figure 9b shows for Exp2a,

325 2b and 2c, can lead to significant changes in $p(K_{imp})$ with larger β corresponding to higher probability of larger K_{imp}, namely,

326 high saltation bombardment intensity. In Exp3a and 3b, u_{2m} (mean wind 2m height) is set to 7.3ms^{-1} and the surface sensible

327 heat flux, H, to -100 and 400 Wm^{-2}. Figure 9c shows that $p(K_{imp})$ differs with larger K_{imp} in unstable conditions.

328 Table 2: Numerical experiments for saltation bombardment intensity. For all experiments, $z_0 = 0.48$mm, $C_0 = 5$, $C_1 = 2$ and $\rho_p = 2650$kgm^{-3}.

Exp	u_* (ms^{-1})	L (m)	d (μm)	β
Exp1a, 1b, 1c	0.35	∞, 30, -9	100	1.0
Exp2a, 2b	0.35	30	200	0.75, 1
Exp2c	0.35	-9	200	1.25
Exp3a, 3b	$u_{2m}=7.3$	H=-100; 400 Wm^{-2}	200	1

329

330   To summarize, the numerical experiments suggest that the PDF of the particle initial velocity significantly influences the
331   saltation bombardment intensity, and saltating particles in unstable ABL impact the surface with larger kinetic energy than in
332   stable ABL. This is the result seen in Figure 8, i.e., saltation in Event-10 was more fully developed than in Event-11. The
333   more fully developed saltation in unstable ABL increases saltation bombardment intensity and hence the release of finer dust
334   particles, seen in Figure 6.

4.2 Influence of Surface Condition on Dust PSD

336   A detailed analysis of Event-12 (Figure 10) reveals that the dependency of dust PSD on friction velocity and ABL stability
337   is made complicated by soil surface conditions. To analysis how dust PSD evolved during the event, we divide Event-12 that
338   lasted ~5.5 hours into 11 half hourly time sections labelled as S1, S2 etc. For each section the dust PSD is averaged over
339   time and plotted in Figure 10c. Figure 10a shows the time series of Q, w_* and u_*, and Figure 11b the time series of 2cm soil
340   temperature and soil moisture. For the whole event, the ABL was unstable, with w_* fluctuating around $1.64 \pm 0.12 \text{ms}^{-1}$.
341   Initially (e.g. S1 and S2), u_* was relatively large, exceeding 0.4ms^{-1} at times, but then eased to around 0.3ms^{-1}. Q generally
342   followed the variations of u_*. Yet, the dust PSD showed a systematic shift from coarser to finer particles, as the event
343   progressed. The dust PSD dependency on u_* of Event-12 does not conform with the results for Event-11 (Figure 6) and the
344   overall results (Figure 4a). Ishizuka et al. (2008) noticed that prior to Event-12, weak rainfall occurred (R4, Figure 5b) and
345   consequently, weak crusts formed on the soil surface. Apparently, the lightly crusted surface prevented the emission of fine
346   dust particles in the early stages of Event-12. As the event progressed, soil temperature increased, soil moisture decreased
347   (Figure 10b) and the saltation during the early stages caused the destruction of the crusts and the amount of fine dust
348   particles available for emission increased. These are the most likely reasons for why in the later stages of Event-12, an
349   increased fraction of fine dust was released, although the atmospheric stability did not significantly change and u_* actually
350   reduced.

351
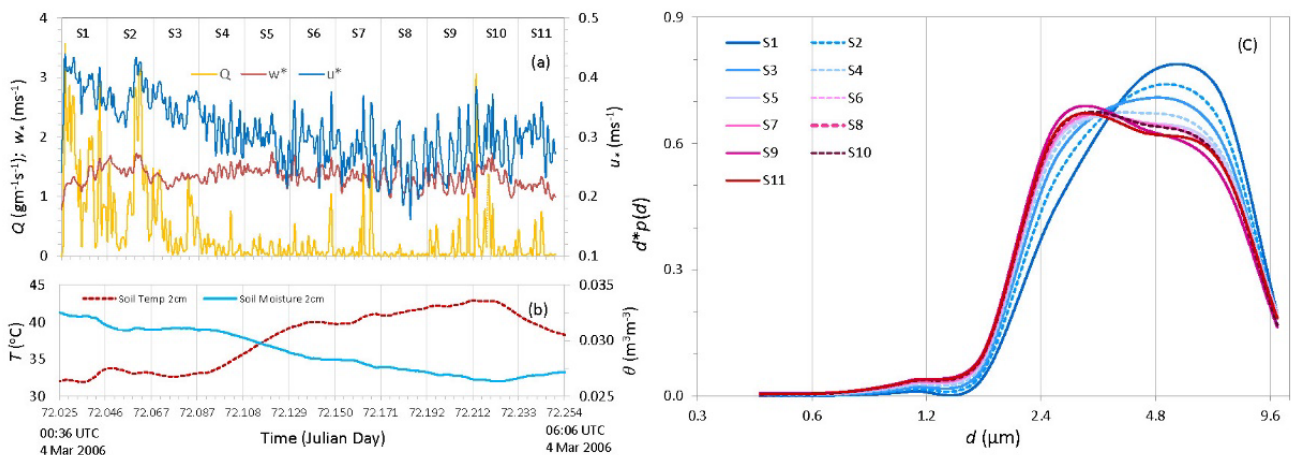
Figure 10. (a) Time series of streamwise saltation flux, Q ($gm^{-1}s^{-1}$), convective scaling velocity, w_* (ms^{-1}), and friction velocity, u_* (ms^{-1}), for Event-12. The time span of Event-12 is divided into 11 half-hourly sections, labelled as S1, S2 etc. (b) As (a), but for soil temperature, T (^oC), and soil moisture, θ (m^3m^{-3}), both at 0.02m depth. (c) Dust PSDs averaged over section S1, S2 etc.

4.3 Uncertainties

We now discuss several issues related to the uncertainties of the analysis. First, the approximation of emission-dust PSD with airborne-dust PSD measured at some height above ground causes uncertainties, because airborne-dust PSD is height dependent as consequence of the dust-transport processes (e.g. diffusion and deposition) in the atmosphere, which are both particle-size and turbulence-property dependent. As our understanding of these processes is not complete and dust measurements have inaccuracies, a careful selection of the data for the analysis is necessary. Figure 11 shows a comparison of Event-10 averaged airborne-dust PSDs at 1m and 3.5m. Ishizuka et al. (2014) suggested to exclude the 2m-OPC data, because they do not correlate well with the 1m- and 3.5m-OPC data. The PSDs derived from the 2m-OPC data do show unexpected differences in comparison to those from the 1m- and 3.5m-OPC data. We thus have excluded the 2m-OPC data from our analysis. The PSDs derived from the 1m- and 3.5m-OPC data somewhat differ, with the peak particle size shifted by about two microns, i.e., airborne-dust PSD has a noticeable change with height. This also implies that it would be very difficult to compare airborne-dust PSD measured at different locations and under different conditions without a well-established framework equivalent to the Monin-Obukhov similarity theory.

Also shown in Figure 11 is the Event-10 averaged emission-flux PSD calculated using Equation (3a). Dust fluxes for different particle size bins are calculated using the 3.5m- and 1m-OPC data with the gradient method (Gillette et al. 1972) and corrections (Shao et al. 2011). As dust flux is proportional to the negative gradient of dust concentration, emission-flux PSD basically describes how dust-concentration gradient [in our case $-(c_{3.5m} - c_{1m})$] depends on particle size.

374
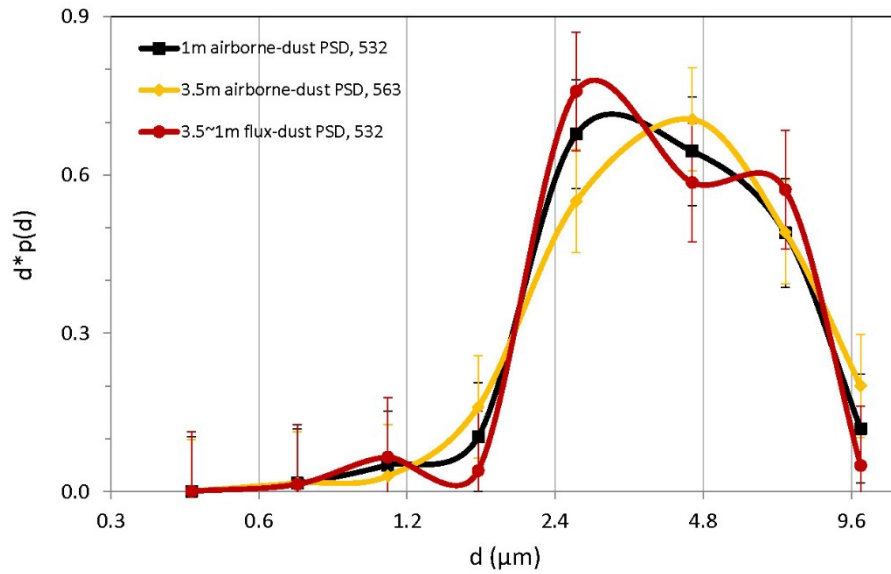
Figure 11: JADE Event-10 averaged airborne-dust PSD measured at 1m (532 one-minute samples) and 3.5m (563 one-minute samples) using OPCs. Also shown are standard-error bars. For comparison, Event-10 averaged (over 532 one-minute samples) emission-flux PSDs calculated using Equation (3a) is plotted.

Although dust PSDs derived from 1m-OPC and 3.5m-OPC data differ, qualitatively they show similar dependencies of dust PSD on u_* and w_*. Figure 12a compares the averaged dust PSDs for two u_* categories using the 1m-OPC and 3.5m-OPC data. For both cases, the dust PSD dependency on u_* is visible. Figure 12b compares the averaged dust PSD for a given u_* category (0.35~0.45ms^{-1}) under stable and unstable conditions. Again, both the 1m-OPC and 3.5m-OPC dust PSDs show dependency on w_*.
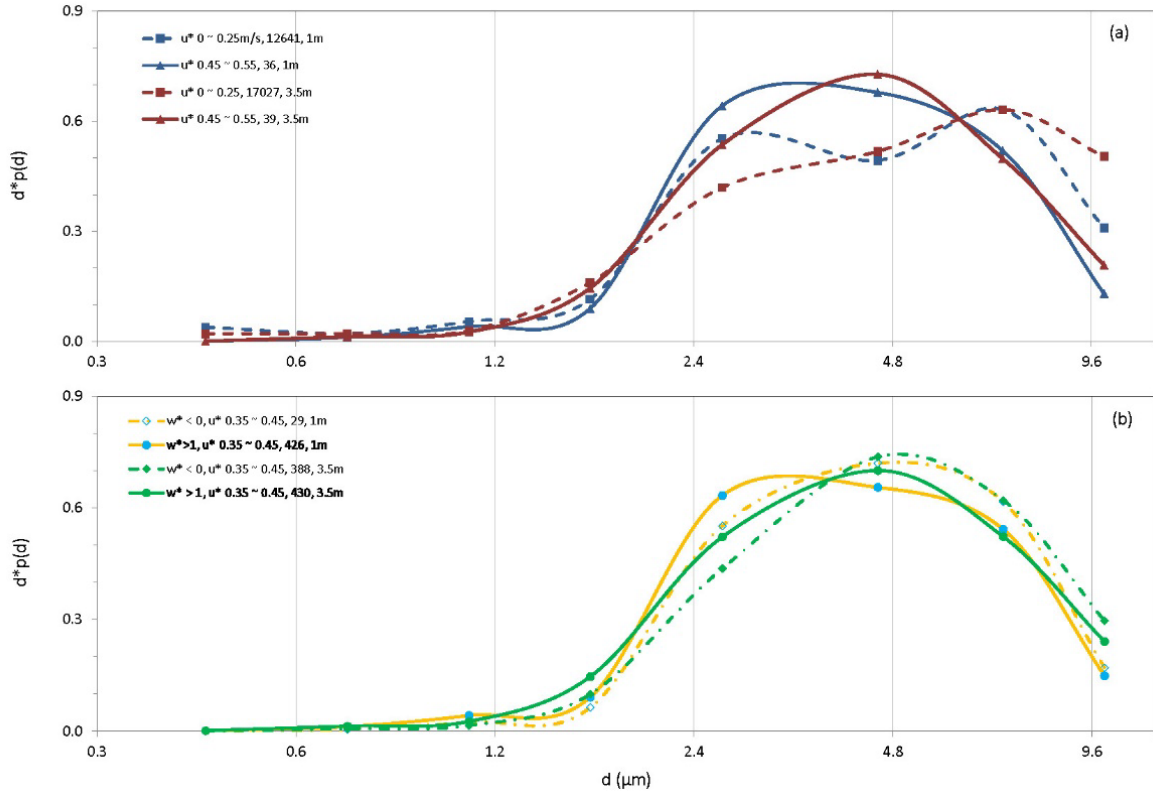
383

384 Figure 12: (a) JADE averaged airborne-dust PSD measured at 1 and 3.5m for two u_* categories. (b) As (a) but for one u_*

385 category and two different stabilities.

386

387   It needs to be clarified whether using 1-minute averages of shear stress, saltation flux and dust flux are appropriate for the

388 study. Related to this question are two inter-wined yet somewhat different scaling issues, namely, (1) the scaling of turbulent

389 flux and the corresponding mean variable of boundary-layer turbulent flow (i.e. the flux and gradient relationship); and (2)

390 the scaling of aeolian fluxes and atmospheric forcing (i.e. saltation/dust-emission intermittency). It is usual in boundary-layer

391 meteorology to compute a turbulent flux from the profile of the corresponding mean quantity, e.g., mean shear stress from

392 mean wind profile, and the time interval for the mean is typically 15 to 30 minutes such that the assumptions of horizontal

393 homogeneity and stationarity commonly made in boundary-layer studies are met. This issue is not yet fully resolved even in

394 boundary-layer studies. For example, large-eddy models (with spatial resolution of several meters and temporal resolution of

395 seconds) frequently use the Monin-Obukhov similarity functions to estimate sub-grid surface stress from the grid-resolved

396 speed. In this study, we distinguish the 1-min averages of u_* from the mean shear stress of the boundary-layer flow to

397 emphasize the importance of shear stress fluctuations. The problem how to scale aeolian fluxes is not new (e.g. Shao and

398 Mikami, 2005). Dupont (2020) has a dedicated paper on this problem and stated that u_* is a suitable scaling parameter for

399 dust flux over usual 15~30-min time intervals, but at smaller time resolution, wind becomes more relevant to scale dust

400 fluxes, a conclusion similar to that reached in Sterk et al. (1998). The studies of Stout and Zobeck (1997) and Sterk et al.
401 (1998), and more recently Klose and Shao (2012) and Klose et al. (2014), all pointed to the importance of taking
402 instantaneous shear stress into consideration of aeolian dynamics. As Shao (2008, p203-205) explains, $\tau_{inst} \sim U'^2$, where τ_{inst}
403 is instantaneous shear stress and U' instantaneous wind speed. The argument of Shao (2008) reasonably well explains the
404 conclusions of Sterk et al. (1998) and Dupont (2020). Liu et al. (2018, Figure 7) analysed co-spectrum of saltation flux and
405 shear stress and showed that they have a correlation peak at 2×10^{-3}Hz, corresponding to gusts/large eddies of around 10
406 minutes in turbulent flows. These considerations suggest that to average shear stress and aeolian fluxes over one minute is
407 appropriate and has the advantage of showing how dust emission is related to turbulence. We have emphasised throughout
408 this paper that turbulence is key to understanding the dependency of dust PSD on ABL stability, because most essential
409 difference among ABLs of different stability are the intensity and structure of turbulence.

410   As far as averaged dust PSDs are concerned, we have compared the dust PSDs averaged for different u_* categories using
411 1-minute averaged data and 10-minute averaged data. The results are almost the same.

5 Conclusions

413 Using JADE data, we showed that dust PSD is dependent on friction velocity u_*. This finding is consistent with the wind-
414 tunnel study of Alfaro et al. (1997). The JADE data support the claim that dust PSD is saltation-bombardment dependent and
415 does not support the hypothesis that dust PSD is invariant.

416   The JADE data show that dust PSD, as well as saltation PSD, also depends on ABL stability. This finding is consistent
417 with the results of Khalfallah et al. (2020). Dust PSD is dependent on ABL stability for two reasons. First, u_* is a stochastic
418 variable and the PDF of u_* profoundly influences the magnitude of saltation flux, Q, because of the non-linear relationship
419 between Q and u_*. With fixed u_* mean, a larger u_* variance corresponds to a larger Q. Unstable ABL has in general larger u_*
420 variances which generate stronger saltation bombardment and produce the emission of finer dust particles. Second, in
421 unstable ABL, turbulence is generally stronger and in strong turbulent flows, the proportion of saltation particles with large
422 impacting kinetic energy is larger than in weak turbulent flows. Consequently, saltation in unstable ABLs is more fully
423 developed and saltation bombardment has higher intensity.

424   The dependencies of dust PSD on u_* and ABL stability are ultimately attributed to the statistic behaviour of u_*, i.e., its
425 PDF $p(u_*)$, or more simply its mean and variance. These dependencies point to the same fact that, for a given soil, saltation
426 bombardment plays a determining role for the dust PSD. Stronger saltation causes the emission of finer dust.

427   The dependency of dust PSD on u_* and ABL stability is made complicated by soil surface condition. In the case of strong
428 saltation and very weak surface binding, the dust PSD dependency on u_* may become less obvious. In the case of strong
429 surface binding, dust emission in certain size ranges may be prohibited.

430

431 *Data availability*. Data can be accessed by contacting the corresponding authors.

432

Author contributions. Yaping Shao performed the data analyses and drafted the manuscript. Jie Zhang and Ning Huang contributed to the conception of the study, the data analysis and the writing of the manuscript. Masahide Ishizuka, Masao Mikami and John Leys conceived, designed and performed the experiments and helped finalize the paper.

436

Competing interests. The authors declare that they have no conflict of interest.
438
Acknowledgments. We thank the National Key Research and Development Program of China (2016YFC0500901), the National Natural Foundation of China (11602100, 11172118) and the Fundamental Research Funds for the Central Universities (lzujbky-2020-cd06) for support. The JADE project was supported by Kakenhi, Grants-in-Aid for Scientific Researches (A) from the Japan Society for the Promotion of Science (Nos. 17201008 and 20244078) and the Lower Murray-Darling Catchment Management Authority. We are grateful to the three referees for their constructive comments and to Dr. Sylvain Dupont and Dr. Jasper Kok for helpful discussions.

References

Albani, S., Mahowald, N. M., Perry, A. T., Scanza, R. A., Zender, C. S., Heavens, N. G., Maggi, V., Kok, J. F. and Otto-Bliesner, B. L., Improved dust representation in the Community Atmosphere Model. J. Adv. Model. Earth Syst., 6: 541–570, doi:10.1002/2013MS000279, 2014.

Alfaro, S. C., Gaudichet, A., Gomes, L. and Maille, M., Modeling the size distribution of a soil aerosol produced by sandblasting. J. Geophys. Res-Atmos., 102: 11239-11249, https://doi.org/10.1029/97JD00403, 1997.

Astrom, J. A., Statistical models of brittle fragmentation. Adv. Phys, 55: 247-278. https://doi.org/10.1080 /00018730600731907, 2006.

Businger, J. A., Wyngaard, J. C., Izumi, J. and Bradley, E. F., Flux-Profile Relationships in the Atmospheric Surface Layer, J. Atmospheric Sci., 28(2): 181–189. https://doi.org/10.1175/1520-0469(1971)028<0181:FPRITA>2.0.CO;2, 1971.

Csanady (1963, Turbulent Diffusion of Heavy Particles in the Atmosphere. J. Atmos. Sci. 20, 201–208).Csanady, G. T., Turbulent Diffusion of Heavy Particles in the Atmosphere. J. Atmos. Sci., 20: 201–208, https://doi.org/10.1175/1520-0469(1963)020<0201:TDOHPI>2.0.CO;2, 1963.

Dupont, S., Scaling of dust flux with friction velocity: time resolution effects. J. Geophys. Res-Atmos., 125, e2019JD031192. https://doi.org/10.1029/2019JD031192, 2020.

Durána, O., Andreotti, B. and Claudin, P., Numerical simulation of turbulent sediment transport, from bed load to saltation. Physics of Fluids, 24(10): 709-737, https://doi.org/10.1063/1.4757662, 2012.

Gillette, D. A., Blifford, I. H. and Fenster, C. R., Measurements of aerosol size distributions and vertical fluxes of aerosols on land subject to wind erosion. J. Appl. Meteor., 11: 977-987, https://doi.org/10.1175/1520-0450(1972)011<0977:MOASDA>2.0.CO;2., 1972.

465 Gillette, D. A., Blifford, I. H. and Fryrear, D. W., Influence of wind velocity on size distributions of aerosols generated by
466   wind erosion of soils. J. Geophys. Res., 79: 4068-4075. https://doi.org/10.1029/JC079i027p04068, 1974.

467 Gillette, D. A., Production of dust that may be carried great distances. Geol. Soc. Am., 186, 11 – 26.
468   https://doi.org/10.1130/SPE186-p11, 1981.

469 Giorgi, F., Coppola, E., Solmon, F., Mariotti, L., Sylla, M. B., Bi, X., Elguindi, N., Diro, G. T., Nair, V., Giuliani, G.,
470   Turuncoglu, U. U., Cozzini, S., Güttler, I., O'Brien, T. A., Tawfik, A. B., Shalaby, A., Zakey, A. S., Steiner, A. L., Stordal,
471   F., Sloan, L. C. and Brankovic, C., RegCM4: model description and preliminary tests over multiple CORDEX domains.
472   Clim. Res., 52, 7–29. doi: 10.3354/cr01018, 2012.

473 Ishizuka, M., Mikami, M., Leys, J. F., Yamada, Y., Heidenreich, S., Shao, Y. and McTainsh, G. H., Effects of soil moisture
474   and dried raindroplet crust on saltation and dust emission. J. Geophys. Res-Atmos., 113: D24212. https://doi.org/10.1029/
475   2008JD009955, 2008.

476 Ishizuka, M., Mikami, M., Leys, J. F., Shao, Y., Yamada, Y. and Heidenreich, S., Power law relation between size-resolved
477   vertical dust flux and friction velocity measured in a fallow wheat field. Aeolian Research, 12: 87–99,
478   https://doi.org/10.1016/j.aeolia.2013.11.002, 2014.

479 Kaimal, J. C. and Finnigan J. J., Atmospheric Boundary Layer Flows: Their Structure and Measurements. Bound.-Lay.
480   Meteorol., 72: 213–214. https://doi.org/10.1007/BF00712396, 1995.

481 Khalfallah, B., Bouet, C., Labiadh, M., Alfaro, S., Bergametti, G., Marticorena, B., Lafon, S., Chevaillier, S., Féron, A.,
482   Hease, P., Henry-des-Tureaux, T., Sekrafi, S., Zapf, P. and Rajot, J. L., Influence of atmospheric stability on the size-
483   distribution of the vertical dust flux measured in eroding conditions over a flat bare sandy field. J. Geophys.l Res-Atmos.,
484   125, e2019JD031185. https://doi.org/10.1029/2019JD031185, 2020.

485 Klose, M. and Shao, Y., Stochastic parameterization of dust emission and application to convective atmospheric conditions.
486   Atmos. Chem. Phys., 12(1): 3263-3293, https://doi:10.5194/acp-12-7309-2012, 2012.

487 Klose, M., Shao, Y., Li, X., Zhang, H., Ishizuka, M., Mikami, M. and Leys, J. F., Further development of a parameterization
488   for convective turbulent dust emission and evaluation based on field observations. J. Geophys. Res-Atmos., 119: 10,441–
489   10. https://doi.org/10.1002/2014JD021688, 2014.

490 Kok, J. F., Does the size distribution of mineral dust aerosols depend on the wind speed at emission? Atmos. Chem. Phys.,
491   11: 10149-10156. https://doi.org/10.5194/acp-11-10149-2011, 2011a.

492 Kok, J. F., A scaling theory for the size distribution of emitted dust aerosols suggests climate models underestimate the size
493   of the global dust cycle. Proc. Natl. Acad. Sci. USA, 108(3): 1016-1021. https://doi.org/10.1073/pnas.1014798108, 2011b.

494 Kok, J. F., Parteli, E. J., Michaels, T. I. and Karam, D. B., The physics of wind-blown sand and dust. Reports on Progress in
495   Physics Physical Society, 75(10): 106901, https://doi.org/10.1088/0034-4885/75/10/106901 , 2012.

496 Laurent, B., Marticorena, B., Bergametti, G., Mei, F., Modeling mineral dust emissions from Chinese and Mongolian deserts.
497   Global Planet Change, 52: 121–141, https://doi.org/10.1016/j.gloplacha.2006.02.012, 2006.

498 Li, G., Zhang, J., Herrmann, H, J., Shao, Y. and Huang, N. Study of Aerodynamic Grain Entrainment in Aeolian Transport,

499   Geophys. Res. Lett.,47(11), https://doi.org/10.1029/2019GL086574, 2020.

500 Liu, D., Ishizuka, M., Mikami, M., and Shao, Y., Turbulent characteristics of saltation and uncertainty of saltation model

501   parameters, Atmos. Chem. Phys., 18: 7595–7606, https://doi.org/10.5194/acp-18-7595-2018, 2018.

502 Lu, H. and Shao, Y., A new model for dust emission by saltation bombardment. J. Geophys. Res-Atmos., 104: 16827-

503   16842. https://doi.org/10.1029/1999JD900169, 1999.

504 Marticorena, B., Bergametti, G., Aumont, B., Callot, Y., N'Doume, C. and Legrand, M., Modeling the atmospheric dust

505   cycle: 2. Simulation of Saharan dust sources. J. Geophys. Res., 102D(4): 4387–4404,

506   https://doi.org/10.1029/96JD02964,1997.

507 Martin, R. L. and Kok, J.F., Wind-invariant saltation heights imply linear scaling of aeolian saltation flux with shear stress.

508   Science Advances, Vol. 3, no. 6, e1602569, DOI: 10.1126/sciadv.1602569, 2017.

509 Mikami, M., Yamada, Y., Ishizuka M., Ishimaru, T., Gao, W. and Zeng, F., Measurement of saltation process over gobi and

510   sand dunes in the Taklimakan desert, China, with newly developed sand particle counter. J. Geophys. Res-Atmos., 110,

511   D18S02, https://doi.org/10.1029/2004JD004688, 2005.

512 Owen, R. P., Saltation of uniform grains in air. J. Fluid. Mech., 20: 225–242, https://doi.org/10.1017/S0022112064001173,

513   1964.

514 Pisso, I., Sollum, E., Grythe, H., Kristiansen, N., Cassiani, M., Eckhardt, S., Arnold, D., Morton, D., Thompson, R. L.,

515   Groot Zwaaftink, C. D., Evangeliou, N., Sodemann, H., Haimberger, L., Henne, S., Brunner, D., Burkhart, J. F.,

516   Fouilloux, A., Brioude, J., Philipp, A., Seibert, P., and Stohl, A., The Lagrangian particle dispersion model FLEXPART

517   version 10.4. Geosci. Model Dev., 12: 4955–4997, https://doi.org/10.5194/gmd-12-4955-2019, 2019.

518 Raupach, M.R., Drag and drag partition on rough surfaces. Boundary-Layer Meteorol., 60, 375–395.

519   https://doi.org/10.1007/BF00155203, 1992.Reid, J. S., Reid, E. A., Walker, A., Piketh, S., Cliff, S., Al Mandoos, A., Tsay,

520   S.-C. and Eck, T. F., Dynamics of southwest Asian dust particle size characteristics with implications for global dust

521   research. J. Geophys. Res-Atmos., 113, D14212. https://doi.org/10.1029/2007JD009752, 2008.

522 Rice, M. A., Willetts, B. B. and McEwan, I. K., An experimental study of multiple grain-size ejecta produced by collisions

523   of saltating grains with a flat bed. Sedimentology, 42: 695-706. https://doi.org/10.1111/j.1365-3091.1995.tb00401.x, 1995.

524 Rice, M. A., Willetts, B. B. and McEwan, I. K., Observations of collisions of saltating grains with a granular bed from high-

525   speed cine-film. Sedimentology, 43: 21-31. https://doi.org/10.1111/j.1365-3091.1996.tb01456.x, 1996.

526 Rosenberg, P. D., Parker, D. J., Ryder, C. L., Marsham, J. H., Garcia-Carreras, L., Dorsey, J. R., Briiks, I. M., Dean A. R.,

527   Crosier J., McQuaid, J. B. and Washington, R., Quantifying particle size and turbulent scale dependence of dust flux in the

528   Sahara using aircraft measurements, J. Geophys. Res-Atmos., 119: 7577–7598. https://doi.org/10.1002/2013JD021255,

529   2014.

530 Shao, Y., A model for mineral dust emission. J. Geophys. Res-Atmos., 106: 20239-20254. https://doi.org/10.1029/

531   2001JD900171, 2001.

532 Shao, Y., Simplification of a dust emission scheme and comparison with data. J. Geophys. Res., 109, https://doi.org/10.1029/2003JD004372, 2004.

534 Shao, Y., Physics and Modelling of Wind Erosion. Springer, https://doi.org/10.1007/978-1-4020-8895-7, 2008.

535 Shao, Y., Ishizuka, M., Mikami, M. and Leys, J. F., Parameterization of size-resolved dust emission and validation with measurements. J. Geophys. Res.-Atmos., 116, D08203, https://doi.org/10.1029/2010JD014527, 2011.

537 Shao, Y. and Mikami, M., Heterogeneous Saltation: Theory, Observation and Comparison. Boundary-Layer Meteorol, 115: 359–379, https://doi.org/10.1007/s10546-004-7089-2, 2005.

539 Shao, Y., Raupach, M. R. and Findlater, P. A., Effect of saltation bombardment on the entrainment of dust by wind. J. Geophys. Res.-Atmos., 98: 12719-12726. https://doi.org/10.1029/93JD00396, 1993.

541 Sow, M., Alfaro, S., Rajot, J. L., Marticorena, B., Size resolved dust emission fluxes measured in Niger during 3 dust storms of the AMMA experiment. Atmos. Chem. Phys., 9, 3881-3891, https://doi.org/10.5194/acp-9-3881-2009, 2009.

543 Sterk G., Jacobs A.F.G. and van Boxel J.H., The effect of turbulent flow structures on saltation sand transport in the atmospheric boundary layer. EARTH SURF. PROC. LAND., 23: 877 – 887, https://doi.org/10.1002/(SICI)1096-9837(199810)23:10<877::AID-ESP905>3.0.CO;2-, 1998.

546 Stout, J.E., Zobeck, T.M., Intermittent saltation. Sedimentology, 44: 959–970, https://doi.org/10.1046/j.1365-3091.1997.d01-55.x, 1997.

548 Stull, R. B., An Introduction to Boundary Layer Meteorology. Kluwer Academic Publishers, Boston. http://dx.doi.org/10.1007/978-94-009-3027-8, 1988.

550 Ungar, J.E. and Haff, P.K., Steady state saltation in air. Sedimentology, 34: 289–299, https://doi.org/10.1111/j.1365-3091.1987.tb00778.x, 1987.

552 Walklate, P.J., A random-walk model for dispersion of heavy particles in turbulent air flow. Boundary-Layer Meteorol 39: 175–190, https://doi.org/10.1007/BF00121873, 1987.

554 Wang, L., and D. E. Stock, Dispersion of Heavy Particles by Turbulent Motion. J. Atmos. Sci., **50**: 1897–1913, https://doi.org/10.1175/1520-0469(1993)050<1897:DOHPBT>2.0.CO;2, 1993.

556 Webb, N. P., Chappell, A., LeGrand, S. L., Ziegler, N. P., Edwards, B. L., A note on the use of drag partition in aeolian transport models. Aeolian Research, 42, https://doi.org/10.1016/j.aeolia.2019.100560, 2020.

558 Yahaya, S., Frangi, J. P. and Richard, D. C., Turbulent characteristics of a semiarid atmospheric surface layer from cup anemometers - Effects of soil tillage treatment (Northern Spain). Annales Geophysicae, 21: 2119-2131. https://doi.org/10.5194/angeo-21-2119-2003, 2003.

561 Zender, C.S., Bian, H., Newman, D., Mineral Dust Entrainment and Deposition (DEAD) model: Description and 1990s dust climatology. J. Geophys. Res., 108: 4416, https://doi.org/10.1029/2002JD002775, 2003.